

Electroacupuncture at BL15 improved arrhythmia-induced cardiomyopathy associated with restoring disordered conduction and calcium handling

Shengxuan Sun^{1,2}, Jing Huang², Yijun Hu^{1,3}, Yang Su², Huanhuan Yu^{1,3}, Feng Guo^{1,3}, Meng Zhang^{1,3,4}, Yucen Xia^{1,3,4}, Lin Yao^{1,3,4}, Taiyi Wang^{1,3,4,*}, Yongjun Chen^{1,3,4,*}

¹Institute of Acupuncture and Moxibustion, Shandong University of Traditional Chinese Medicine, Jinan, China; ²South China Research Center for Acupuncture and Moxibustion, Medical College of AcuMoxi and Rehabilitation, Guangzhou University of Chinese Medicine, Guangzhou, China; ³Shandong Key Laboratory of Innovation and Application Research in Basic Theory of Traditional Chinese Medicine, Shandong University of Traditional Chinese Medicine, Jinan, China; ⁴Key Laboratory of Traditional Chinese Medicine Classical Theory, Ministry of Education, Shandong University of Traditional Chinese Medicine, Jinan, China

Abstract

Objective: Arrhythmia-induced cardiomyopathy (AIC) is a reversible dilated cardiomyopathy induced by rapid or irregular heartbeat. Acupuncture has a long history of use in the treatment of cardiac diseases, and Xinshu (BL15) is a key acupoint. However, the underlying mechanism of acupuncture at BL15 in the treatment of AIC has not yet been elucidated.

Methods: AIC was induced in adult male Sprague-Dawley (SD) rats by continuous administration of acetylcholine (ACh)-CaCl₂ and treatment with electroacupuncture (EA) at bilateral BL15. Echocardiography was used to evaluate cardiac function; the rotarod test for motor coordination and performance; hematoxylin and eosin (HE) staining for the morphology of ventricles; electrocardiogram for susceptibility, inducibility, and duration of atrial fibrillation (AF); and electrical and optical mapping in isolated rat hearts maintained by the Langendorff perfusion system for electrical conduction and intracellular handling, respectively. Reverse transcription quantitative polymerase chain reaction (RT-qPCR) and Western blotting were used to determine the levels of cardiac conduction and intracellular calcium-handling proteins in the ventricle.

Results: The results showed that EA improved the ejection factor and morphological indices on echocardiography, restored motor coordination and performance, and alleviated ventricular dilation and AF onset. EA alleviates atrial conduction disorders, shortens APD₈₀, and decreases calcium handling in rats with AIC. Cx43 was downregulated and CaMKII was upregulated, and both effects were reversed by EA treatment.

Conclusion: Our study provides a novel AIC model with abnormal electrical propagation and calcium handling that can be protected by EA at BL15. This potential mechanism may be associated with the modulation of Cx43 and CaMKII expression.

Keywords: Arrhythmia-induced cardiomyopathy, BL15, Calcium handling, Cardiac conduction, Electroacupuncture

Introduction

Arrhythmia-induced cardiomyopathy (AIC) is a specific type of dilated cardiomyopathy characterized by left ventricular systolic dysfunction induced by rapid or irregular heart rhythm^[1]. AIC was observed in 58% to 88% of atrial fibrillation (AF) patients, 38% of patients with premature ventricular contraction (PVC) patients and 8.3% to 10% of adult atrial tachycardia patients^[2-5]. An increasing number of clinical studies have shown that the highest proportion of AIC cases is caused by AF^[6-7]; however, the underlying pathology of AIC has not been

fully elucidated^[2,8]. Current therapeutic strategies for AIC primarily aim to correct cardiac electrophysiological abnormalities^[2]. Standard treatments include antiarrhythmic drugs, such as amiodarone (Amio), and catheter ablation to eliminate ectopic pacemaker foci. However, these approaches have several limitations. Long-term Amio use can lead to adverse effects, including bradycardia and hemorrhagic complications, and patients who undergo catheter ablation often experience high recurrence rates^[9-11]. Although these interventions alleviate arrhythmic symptoms and improve cardiac function,

Shengxuan Sun, Jing Huang, and Yijun Hu contributed equally to this work.

*Corresponding author. Yongjun Chen, E-mail: chen Yongjun@sdutcm.edu.cn; Taiyi Wang, E-mail: wangtaiyi@sdutcm.edu.cn.

How to cite this article: Sun SX, Huang J, Hu YJ, Su Y, Yu HH, Guo F, Zhang M, Xia YC, Yao L, Wang TY, Chen YJ. Electroacupuncture at BL15 improved arrhythmia-induced cardiomyopathy associated with restoring disordered conduction and calcium handling. *Acupunct Herb Med* 2025;5(3):338-351. doi: 10.1097/HM9.000000000000169

Received 12 February 2025 / Accepted 23 August 2025

Copyright © 2025 Tianjin University of Traditional Chinese Medicine. This is an open-access article distributed under the terms of the Creative Commons Attribution-Non Commercial-No Derivatives License 4.0 (CCBY-NC-ND), where it is permissible to download and share the work provided it is properly cited. The work cannot be changed in any way or used commercially without permission from the journal.

they do not sufficiently target structural remodeling, which is a key pathological mechanism underlying AIC recurrence and progression to heart failure. Therefore, there is an urgent need to develop new therapeutic strategies that not only improve clinical outcomes and minimize adverse events but also reverse pathological cardiac remodeling through multi-target mechanisms.

AIC has two major pathological manifestations: arrhythmia and cardiomyopathy. One of the most crucial drivers of arrhythmia, especially AF, is abnormal electrical propagation, such as slowing of conduction velocity (CV) or an abnormal excitation sequence (ectopic trigger or re-entry)^[12–15]. Furthermore, the depolarization and repolarization of atrial cardiomyocytes are critical for the inducibility of AF^[16–17]. Notably, reduced cardiac contraction force is related to calcium-handling disorders,^[18] and previous studies have shown that AIC may be associated with defects in myocardial Ca²⁺ transients and Ca²⁺ handling^[19–20]. In addition, the coordinated movement of Ca²⁺ between the cytosol and sarcoplasmic reticulum (SR) is a determinant of cardiac function^[21]. Although both electrical propagation and intracellular calcium handling are suspected to be potential etiologies of AIC^[20,22], direct experimental evidence is lacking. Radical treatment of AIC may require a specific approach to treat both arrhythmia and calcium-handling disorders.

As one of the most common alternative therapies, acupuncture has a long history of use in the treatment of various cardiovascular diseases. The Xinshu acupoint (BL15), located approximately 5 cm lateral to the spine at the T5 level, is one of the most frequently used acupoints for the treatment of cardio- and cerebrovascular diseases, including arrhythmia^[23–24], insomnia^[25], and cerebral-cardiac syndrome^[26], myocardial ischemia^[27], coronary heart disease^[28], and heart failure^[29]. These therapeutic effects may be closely related to the modulation of the autonomic nervous system by acupuncture^[30–31]. Previous studies have reported that BL15 plays a role in the treatment of cardiovascular diseases through mechanisms such as the regulation of autonomous nerve activity and anti-apoptotic effects; however, it is unclear whether BL15 has a therapeutic effect on AIC^[32–33]. In this study, we used a rat model of AIC caused by AF, combined with cardiac electrical and optical mapping technologies, to evaluate the effects of BL15 on AIC *in vivo* and *ex vivo*. Our study not only confirmed that electroacupuncture (EA) treatment at BL15 improved arrhythmias and cardiac dysfunction but also uncovered the possible mechanisms involved in the regulation of electrical conduction and internal calcium disorders in the heart. Our findings revealed that EA effectively treats AIC and may be a promising multi-target therapeutic approach. We propose that future multicenter randomized controlled trials (RCTs) validate the efficacy and safety of EA in clinical populations. These investigations will establish a robust evidence base to inform integrated clinical guidelines that combine traditional Chinese and Western medicine for AIC management.

Materials and methods

Experimental animals

Eight-week-old male Sprague-Dawley (SD) rats weighing approximately 250 g were purchased from Beijing

Spelford Biological Co. Ltd. All animals were randomly assigned to different cages, with four rats per cage, and were given free access to adequate food and water. Room temperature was maintained at (23 ± 1)°C, and relative humidity was maintained at (65 ± 3)% with a 12-hour light/dark circadian cycle. This animal study was approved by the Institutional Animal Care and Use Committee of the Guangzhou University of Chinese Medicine, which is the affiliation of the author, in compliance with the Institutional Animal Care and Use Committee (IACUC) guidelines for the care and use of animals. This study was conducted in accordance with the Animal Research: Reporting of In Vivo Experiments (ARRIVE) guidelines (ethical review approval number: 20201124005).

AIC modeling and treatments

The acetylcholine (ACh)-CaCl₂-induced AIC rat model was modified from a previously described AF rat modeling protocol^[34]. Briefly, ACh (Sigma-Aldrich, Burlington, MA, USA) and CaCl₂ (Sigma-Aldrich) were mixed in saline and stored away from light. Rats in the model group were administered an intravenous injection in the tail with a mixture of 0.01 mL/g (ACh, 66 µg/mL and CaCl₂, 10 mg/mL) daily for 10 consecutive days under anesthesia with 1.5% isoflurane gas (RWD Life Science, Shenzhen, China). The control group received the same volume of 0.9% NaCl solution.

EA treatment

Rats in the EA group were needled bilaterally at the Xinshu acupoints (BL15, located on the back and on the connecting line of the spinal column with a posterior angle of the scapula, 5 mm lateral to the fifth thoracic vertebra). EA stimulation was administered for 20 min/d for 10 consecutive days with a 2 Hz and 2 mA continuous-wave current, as described previously^[35]. Acupuncture needles (0.18 mm diameter × 7 mm length, Suzhou Acupuncture & Moxibustion Appliance Co. Ltd., Suzhou, China) were inserted through the skin approximately 5 to 8 mm at an angle of 30° to 45° leaning toward the tail. The needles were connected to the electrodes and inserted 2 to 3 mm into the stimulated acupoint BL15 (cathode), and the anode point was inserted 4 mm vertically toward the caudal side. Sham EA group rats underwent the same procedure, except for no electrical stimulation at the bilateral BL15 acupoints at a depth of 5 mm and without electrical stimulation. For EA at the Tianshu acupoint (ST25), a pair of needles was bilaterally inserted (3–4) mm into the abdominal muscle layers. To rule out the influence of anesthesia and body fixation, rats from all groups were anesthetized with isoflurane (2%) and fixed on an animal heating pad with adhesive tape in a standard position on their abdomens.

Amio treatment

Amio was administered as previously described^[36]. 50 mg/kg amiodarone hydrochloride (Sanofi, Beijing, China) was administered once daily for 10 days *via* tail vein injection.

Echocardiography

Echocardiography was performed as previously described^[37]. After AIC modeling without EA treatment

for 10 days, the rats were anesthetized with 1.5% isoflurane and fixed on an operative platform. Transthoracic echocardiography was performed using a high-resolution echocardiography machine with a 30 MHz probe. The chest fur was removed using a depilatory paste, and the chest was covered with a fluid-acoustic couplant. The probe was first placed perpendicular to the rat heart and then rotated clockwise by 30° to 45° to determine the left ventricle of the heart. M-mode and two-dimensional images were obtained using a high-resolution small-animal ultrasound system in the short-axis view (Vevo 2100; Visual Sonics, Toronto, ON, Canada). The left ventricular anterior wall diameter (LVAW), left ventricular posterior wall diameter (LVPW), left ventricular internal diameter (LVID), ejection fraction (EF), and fractional shortening (FS) were measured using M-mode images.

Preparation of isolated hearts

We isolated the hearts from rats and maintained their physiological function using the Langendorff perfusion system, as previously described^[38]. Prior to the procedure, the rats were weighed and administered an intraperitoneal injection of heparin sodium (3,125 U/kg). After 15 minutes, anesthesia was induced with isoflurane. Once anesthesia was confirmed, the hearts were rapidly excised and connected to a Langendorff perfusion cannula for perfusion. We performed retrograde perfusion using oxygenated Tyrode's solution, composed of (in mM): 134 NaCl, 4.5 KCl, 0.5 MgCl₂, 2 NaH₂PO₄, 23 NaHCO₃, 1.8 CaCl₂, and 5.5 glucose, equilibrated with a gas mixture of 95% O₂ and 5% CO₂ to maintain a pH of 7.4. The perfusion parameters included constant-pressure retrograde flow (80 cmH₂O), temperature of (37.0 ± 0.2)°C maintained through closed-loop water bath circulation, oxygenation with 95% O₂/5% CO₂, and a flow rate of 8 to 10 mL/min. All hearts were allowed to stabilize for 15 minutes to ensure a steady-state cardiac rhythm before electrophysiological recording.

AF inducibility and effective refractory period (ERP) analysis

Electrophysiological measurements were performed as previously described^[39]. Electrocardiogram (ECG) signals from isolated hearts were recorded using an electrophysiological mapping system (Mapping Lab, EMS64-USB-1003, UK)^[40]. Briefly, a stimulation electrode was inserted into the left atrium of the heart. Two ECG recording electrodes were placed in the right atrium and left ventricle. The pacing current threshold was measured using train stimulation, and the intensity was slowly increased from 1 to 3 mA within 2 ms. The minimum current intensity used to successfully pace the heart was the systolic threshold, and the experimental stimulus current was set to twice the systolic threshold. To determine the inducibility of AF, S1-S1 stimulation was conducted in two steps with identical parameters to induce AF or atrial tachycardia. The duration of the two stimulations at a frequency of 50 Hz, repeated eight times, was used to calculate AF inducibility and AF duration. Next, the ERP was measured using the standard S1-S2 protocol with an intensity that was twice that of

the pacing threshold. We first set a train stimulation of 1 Hz (S1, 5 Hz) repeated 10 times to pace the heartbeat, which was considered the basic stimulation. The interval between S1 and S1 was 100 ms. Stepwise decreasing electrical stimulations of 2 (S2, 5 Hz) were applied. S1 to S2 were repeated 10 times, and the interval of S1 to S2 was set to 60 ms, with a reduction of 5 ms per cycle until S2 could not induce a complete heartbeat signal trace. The last S1 to S2 interval was considered an ERP.

Electrical mapping on ex vivo rat hearts

Electrical mapping was performed using the Langendorff system as previously described^[41] after AF inducibility and ERP detection. An isolated heart ECG was recorded using a pair of ECG electrodes (MappingLab Ltd., Oxford, UK) positioned in the right atrium and left ventricle. After the ECG signal stabilized, a 5 Hz stimulation was used to normalize the heart rate. A 64-channel electrode recording sensor was attached to the left atrial and left ventricular epicardium to record the field potentials at a sampling rate of 10 kHz (EMS64-USB-1003, MappingLab Ltd.). Field potential data were collected using EMapRecord 5.0 software (MappingLab Ltd.) and stored on a computer for subsequent analyses. An isochrone map of epicardial isochronal activation was plotted as the latency between the earliest activated point and each site. Conduction latency, CV, and dispersion index were calculated using EMapScope 5.0 software (MappingLab Ltd.).

Optical mapping on ex vivo rat hearts

Optical mapping was performed under light protection, as previously described^[42-44]. For myocardial staining, 300 µL blebbistatin (10 µM) was injected into the circulation fluid to minimize cardiac contractions. Membrane potential and intracellular calcium handling were measured using voltage- and calcium-sensitive dyes, respectively. Pluronic F127 (20% w/v in dimethyl sulfoxide [DMSO]) was pre-perfused to enhance the efficiency of dye loading, and 100 µL of voltage-sensitive dye RH237 (1 µg/mL) was added. After 10 minutes, the calcium-sensitive dye Rhod-2AM (1 µg/mL) was added to the perfusion to ensure full perfusion of both dyes. Two 530 nm light-emitting diodes (LEDs) (LEDC-2001; MappingLab Ltd.) were used to illuminate the heart after their emissions were bandpass filtered (wavelengths 530 ± 20 nm) to minimize the amount of stray excitation light reaching the dyes. The fluorescent light was passed through a 550 nm long-pass filter and then through a dichroic mirror with a cut-off of 638 nm. Fluorescent light with wavelengths above 638 nm was passed through a 700 nm long-pass filter and then imaged by the camera to record the voltage signals. Fluorescence light below 638 nm was passed through a bandpass filter (585 ± 40 nm) and then imaged using a camera to record the calcium signals (OMS-PCIE-2002; MappingLab Ltd.). The raw spatial resolution was 128 × 128 pixels, the total mapping area was 16 × 16 mm, and the temporal resolution was 900 frames/s. The cameras of the optical mapping system, LED lights, stimulator, and ECG recording were driven simultaneously by an eight-channel transistor-transistor logic

(TTL) analog-to-digital converter and OMapRecord 4.0 software (MappingLab). OMapScope5 software was used to measure OAP and intracellular Ca^{2+} activity, such as rise time, APD_{80} , $CaTD_{80}$, and Ca^{2+} fluorescence amplitude changes for statistical analysis.

Reverse transcription quantitative polymerase chain reaction (RT-qPCR)

Total RNA was isolated from the ventricular tissue using TRIzol reagent (Ambion, Austin, TX, USA) according to the manufacturer's protocol. RNA was reverse-transcribed to cDNA using PrimeScript™ RT Master Mix for qPCR (Takara Bio Inc., Kusatsu, Shiga, Japan). RT-qPCR was performed using a QuantStudio™ 5 Real-Time PCR instrument (Applied Biosystems, Waltham, MA, USA). The primer sequences for the different genes are shown in Table 1. RT-qPCR was performed according to the manufacturer's protocol (Takara), with initial denaturation at 95°C for 30 seconds, followed by 40 consecutive thermal cycles (95°C for 5 seconds; 60°C for 30 seconds) and a final melting curve cycle. Relative mRNA abundance was calculated using the $\Delta\Delta Ct$ method. Each sample was tested at least thrice.

Western blot

Cardiac tissue was homogenized in RIPA Lysis Buffer (Beyotime Biotechnology, Nantong, China) containing 20 μ L/mL of protease and phosphatase inhibitor cocktail (Beyotime). Protein samples were boiled in loading buffer for sodium dodecyl sulfate-polyacrylamide gel electrophoresis (SDS-PAGE) and analyzed by SDS-PAGE. Equal concentrations of solubilized proteins were separated by 10% SDS-PAGE and transferred onto polyvinylidene difluoride (PVDF) membranes. Nonspecific binding to the membranes was prevented by incubation with 5% Blotto (5% nonfat dry milk and 1% Tween-20 in TBS) for at least 1 hour at room temperature (RT). Membranes were then incubated overnight with various primary antibodies at 4°C. The following day, the membranes were washed and incubated for 1 hour with horseradish peroxidase (HRP)-conjugated goat anti-rabbit or goat anti-mouse secondary antibodies at RT. Clarity Western ECL Substrate A and Peroxide Solution B (Vazyme, Nanjing, China) were used for protein band visualization, and Western blot images were captured using a ChemiDoc XRS + imaging system (Bio-Rad Laboratories, Hercules, CA, USA). Protein loading

was normalized to that of GAPDH (1:1,000, 2118S; Cell Signaling Technology, Danvers, MA, USA). The primary antibodies used were anti-CaMKII (1:1,000, GTX52342; GeneTex, Irvine, CA, USA), CaV1.2 (1:1,000, 334 002; Synaptic Systems, Göttingen, Germany), RYR2 (1:500, 19765-1-AP; Proteintech Group, Wuhan, China), Cx40 (1:500, 36-4900; Invitrogen, Waltham, MA, USA), and Cx43 (1:1,000, MAB3067; Sigma-Aldrich).

Statistical analysis

Group differences were assessed using the SPSS Statistics software (version 21.0; IBM Corp., Armonk, NY, USA). Based on the normality of the data distribution, one-way analysis of variance (ANOVA) with Tukey's test was used for multiple comparisons of the data. Unpaired Student *t* tests for two groups and one-way ANOVA with Tukey's test for multiple comparisons were used. Two-way ANOVA followed by the Bonferroni test was applied to APD_{80} , $CaTD_{80}$, and CV using GraphPad Prism 7 (GraphPad Software, Inc., La Jolla, CA, USA). All data are presented as mean \pm standard error of the mean (SEM). Statistical significance was set at $P < 0.05$.

Results

EA improves cardiac function in AIC rats

To determine whether EA has a therapeutic effect on AIC, echocardiography was performed in a modified rat model induced by ACh-CaCl₂ administration for 10 consecutive days (Figure 1A). Representative echocardiographs of each group are shown in Figure 1B. The EF and FS indices decreased in rats after ACh-CaCl₂ administration compared to the control. Notably, both EA at BL15 and Amio treatment reversed these changes, with no effect on Sham EA or EA treatment at ST25 (Figure 1C and D). These results indicate that cardiac output function was decreased in rats with ACh-CaCl₂ administration, which was restored by EA at BL15. Furthermore, indices of left ventricular internal dimension at the end-systole (LVIDs) and left ventricular internal dimension at the end-diastole (LVIDd) were increased, while left ventricular anterior wall in systole (LVAWs), left ventricular anterior wall in diastole (LVAWd), left ventricle posterior wall in systole (LVPWs), and left ventricular posterior wall in diastole (LVPWd) were decreased in rats exposed to ACh-CaCl₂, but all the above indices were reversed by EA treatment at BL15 (Figure 1E–J). Interestingly, rats in the Amio-treated group showed significant changes in LVIDs and

Table 1
qPCR primers

Gene	Upstream primers	Downstream primers
Cacna1c (CaV1.2)	5'-CGCATTGTCAATGACACGATC-3'	5'-CGGCAGAAAGAGCCCTTGT-3'
CaMKII	5'-AAGATGTGCGACCCTGGAATG-3'	5'-TGTAGGCGATGCAGGCTGAC-3'
Cx43	5'-TTGTTTCTGTCCACAGTAAC-3'	5'-GATGAGGAAGGAAGAGAAGC-3'
RyR2	5'-CTGAACATTTTCTCGAAA-3'	5'-TTCAAGCAGTAGTATCCGAT-3'
Cx40	5'-GAAGCAGCCAGAGTGTGAAGAAGCC-3'	5'-TTGCCTACCACGGTCGAGTGCTT-3'
β -actin	5'-CACGGCATTGTAACCAACTG-3'	5'-TCTCAGCTGTGGTGGTGAGG-3'

qPCR: Quantitative polymerase chain reaction.

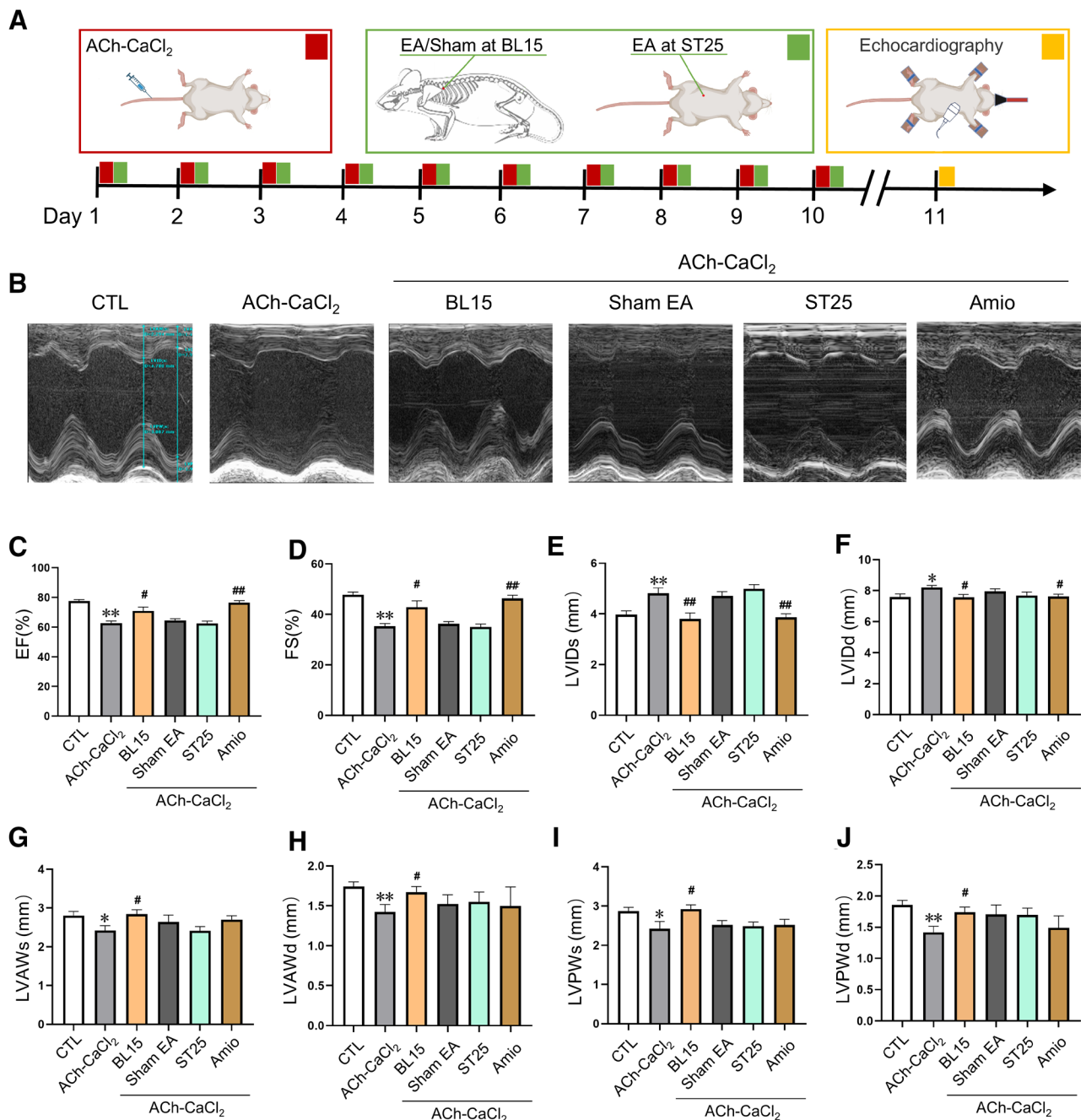


Figure 1. Evaluation of cardiac function in rats exposed to ACh-CaCl₂ with/without EA treatment using echocardiography. (A) Flowchart of the modeling and treatment procedures and time points of ultrasound examination. Rats, 56 days after birth, weighing >300 g, were grouped randomly and treated as follows: control group rats were treated with saline injected into the tail vein once daily for 10 days. Rats in the model group were treated with ACh and CaCl₂ dissolved in saline for AIC modeling. AIC rats treated with EA were treated at the bilateral Xinshu (BL15) acupoints after modeling. The ACh + CaCl₂ + Sham EA group was treated with acupuncture pierced through the skin at a depth of 0.5 mm without electrical stimulation on bilateral Xinshu (BL15) acupoints after modeling. The ACh + CaCl₂ + ST25 group was treated at bilateral Tianshu (ST25) acupoints after modeling. The ACh + CaCl₂ + Amio group was treated with amiodarone after AIC modeling. (B) Representative images of echocardiography examinations. Six groups were assessed in this study, from left to right: control, ACh + CaCl₂, EA treatment, ACh + CaCl₂ + sham EA, ACh + CaCl₂ + ST25, and ACh + CaCl₂ + Amiodarone. (C) %EF, (D) %FS, (E) LVIDs, (F) LVIDd, (G) LVAWs, (H) LVAWd, (I) LVPWs, and (J) LVPWd in all groups as (B) on day 11 (n = 12 in all groups). *P < 0.05, **P < 0.01 vs. control group; #P < 0.05, ##P < 0.01 vs. model group. ACh: Acetylcholine; AIC: Arrhythmia-induced cardiomyopathy; EA: Electroacupuncture; EF: Ejection fraction; FS: Fractional shortening; LVAWd: Left ventricular anterior wall in diastole; LVAWs: Left ventricular anterior wall in systole; LVIDd: Left ventricle internal dimension in diastole; LVIDs: Left ventricle internal dimension in systole; LVPWd: Left ventricular posterior wall in diastole; LVPWs: Left ventricle posterior wall in systole.

LVIDd, but not in the other groups, indicating that Amio may not affect the thickness of the ventricular wall in either the systole or the diastole period compared with rats exposed to ACh-CaCl₂. In contrast, rats in the Sham EA or EA at ST 25 groups did not show any significant changes in the measurements (Figure 1G–J). These data

indicate that continuous administration of ACh-CaCl₂ causes dilated left ventricles and thinner left ventricular walls, and that EA at BL15 has a significant protective effect on cardiac morphology.

We performed the rotarod test to further evaluate the probable motor dysfunction caused by cardiac injury. As

shown in Supplementary Figure S1 (<https://links.lww.com/AHM/A185>), the latency to fall, travel distance, and average velocity decreased compared to those of the control group. EA or Amio treatment significantly restored motor performance indices, but Sham EA failed [Supplementary Figure S1, <https://links.lww.com/AHM/A185>]. To further validate the morphological changes in the left ventricle, we used hematoxylin and eosin (HE) staining to prepare ventricular cross-sections. Consistent with echocardiography [Supplementary Figure S2A–C, <https://links.lww.com/AHM/A186>], the ventricular area was enlarged after ACh-CaCl₂ treatment, as shown by HE staining. Moreover, EA treatment partially reversed ventricular enlargement [Supplementary Figure 2D, <https://links.lww.com/AHM/A186>]. Collectively, these results indicate that ACh-CaCl₂ administration induces cardiac dysfunction and ventricular dilation, which can be prevented by EA treatment at BL15 acupoint.

EA treatment alleviated the onset of arrhythmia at BL15

Improvement of AF is the most effective strategy for treating AIC; therefore, we evaluated whether BL15 improves AF-related phenotypes in rats exposed to ACh-CaCl₂. Next, we performed pseudo-ECG recordings in isolated rat hearts using a Langendorff perfusion system to measure the susceptibility, inducibility, and duration of AF with or without EA at BL15 (Figure 2A). As shown in Figure 2B, rats treated with ACh-CaCl₂ presented an AF-like ECG trace (ie, absence of P-waves, irregular ventricular rate, and ECG baseline showing fibrillatory waves) after 50 Hz pacing, but the control or EA treatment groups did not show this. The results showed that EA treatment significantly reduced the occurrence, inducibility, and duration of AF in the hearts of rats exposed to ACh-CaCl₂ (Figure 2C–E). A shorter ERP can lead to a shorter wavelength, which increases AF inducibility and sustenance duration^[45]. These results indicate that ACh-CaCl₂ administration facilitates the onset of AF. To further elucidate the mechanism by which EA prevents AF, we evaluated the ERP in isolated rat hearts following S1 to S2 stimulation (Figure 2F). The ERP of rats exposed to ACh-CaCl₂ was shorter than that of the control group, whereas EA treatment effectively reversed the shortened ERP (Figure 2G). Collectively, our results indicate that ACh-CaCl₂ administration in rats for 10 consecutive days can induce all AF phenotypes caused by AIC. These results also revealed that EA at BL15 had a protective effect in rats with AIC.

EA treatment improved atrial conduction disorder in AIC rats

Abnormal electrical propagation is one of the most crucial drivers of inducing AF^[46–48]. Next, we performed electrical mapping to evaluate cardiac conduction capability using atrial conduction time (AT), CV, dispersion, and atrioventricular delay time (Figure 3A and B). Compared with control rats, both AT and dispersion in AIC rats were significantly increased, but CV was markedly decreased (Figure 3B–E). In contrast, there was no difference in the atrioventricular delay time between the groups (Figure 3F). Collectively, these results from electrical mapping showed that ACh-CaCl₂ administration

impaired atrial conduction, which was prevented by EA. To confirm these results, optical mapping was used to image the isochrone map of electrical propagation in the atrium (Figure 3G). As shown in Figure 3H and I, a significantly reduced CV was observed in AIC rats compared to that in the control group, which was reversed by EA treatment. Collectively, the results from both electrical and optical mapping revealed that ACh-CaCl₂ administration disrupts electrical signal propagation around cardiomyocytes in the left atrium, whereas EA at BL15 prevents these deficits.

EA treatment prevented repolarization and calcium-handling disorder in atria of AIC rats

Depolarization and repolarization of atrial cardiomyocytes are also critical for inducing arrhythmia, especially AF^[16–17]. Next, we measured the rise time and APD₈₀ of the atrial action potential through optical mapping using the voltage-sensitive dye, RH237 (Figure 4A). As shown in Figure 4B–D, the rise time was significantly decreased in AIC rats compared to that in control rats or AIC rats treated with EA. These results indicate that EA may effectively protect against AF by restoring atrial repolarization. Repolarization is the period when excitation-contraction coupling occurs through intracellular calcium^[49], we further tested intracellular calcium handling through optical mapping with the Ca²⁺-selective dye Rhod 2 AM (Figure 4E). The amplitude of calcium fluorescence in AIC rats was significantly lower than that in the control group or AIC rats treated with EA, whereas the rise time and CaTD₈₀ did not differ between the control, ACh-CaCl₂, or AIC rats treated with EA (Figure 4F–G). These results indicate that calcium handling is associated with the etiology of AIC and may be the underlying mechanism of EA treatment.

EA treatment blocked repolarization and calcium-handling disorder in ventricles

Because the ventricle shares substantial mechanisms of excitation-contraction coupling with the atria, we next recorded the isochrone map and action potential trace of rat ventricles using optical mapping (Figure 5A). The APD₈₀ in the rat ventricle decreased in the ACh + CaCl₂ group (Figure 5B and C) and was restored in AIC rats treated with EA (Figure 5D). Furthermore, we tested intracellular calcium handling in the ventricles using the same methods as for the atria (Figure 5E and F). The results showed that all indices, including rise time, calcium fluorescence amplitude, and CaTD₈₀, were decreased compared with the control, and were recovered by EA treatment at BL15 (Figure 5G–I). Collectively, these results indicate that impaired Ca²⁺ handling in the ventricles caused by AIC can be prevented by EA stimulation at BL15.

EA treatment ameliorated abnormal Cx43 and CaMKII expression in AIC rat hearts

To determine the potential molecular mechanisms, we evaluated the expression of a series of genes and proteins involved in electrical propagation and intracellular calcium handling in the myocardium. Compared with the

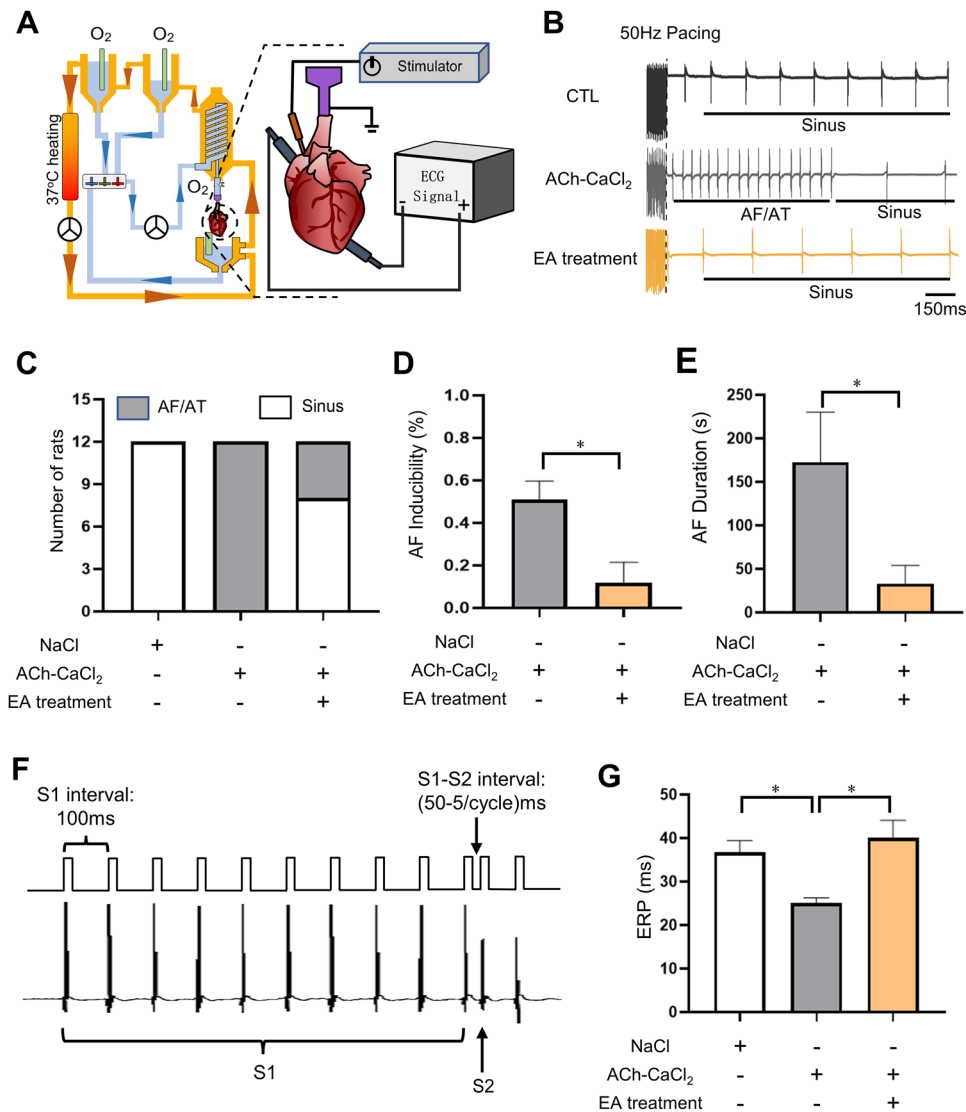


Figure 2. Susceptibility to AF and efficacy of EA in isolated rat hearts. (A) Langendorff perfusion apparatus and ECG recording system. The isolated hearts were cannulated in the tank to perfuse and maintain at physiological temperature, ECG electrodes were placed in the right atrium and left ventricle, and ECGs were recorded after equilibrium. (B) Representative graph of the onset of induced AF and the protective effect of EA treatment in AF hearts. Electrical stimulation with 50 Hz 10 times the threshold current for pacing the rat heart was applied to induce AF, and the inducibility and duration were measured from the ECG recording. (C) Statistics of the number of experimental animals in each group and the number of experimental animals induced with AF by 50 Hz stimulation. (D) Induction rate of AF in the model and treated groups. EA treatment significantly reduced AF inducibility in rat hearts. (E) Duration of AF in the model and treated groups. EA treatment significantly shortened the duration of AF in the rat heart model. (F) Protocol for S1–S2 stimulation. Ten S1 pre-pulses with the same interval were applied before S2 stimulation, and the interval between S2 and S1 decreased gradually until the heart could not be paced by the S2 pulse. The shortest S1–S2 interval was considered the atrial ERP. (G) ERP durations of control, ACh + CaCl₂, and AIC rats treated with EAs. AF modeling shortened the ERP of rat hearts, but EA treatment reversed this effect. $n = 12$ in all groups, $*P < 0.05$. ACh: Acetylcholine; AF: Atrial fibrillation; AIC: Arrhythmia-induced cardiomyopathy; AT: Atrial conduction time; EA: Electroacupuncture; ECG: Electrocardiogram; ERP: Effective refractory period.

control group, the mRNA levels of Cx43, Cx40, RyR2, and CaV1.2 were downregulated in the AIC group. Furthermore, EA treatment blocked the AF-induced decrease in Cx43 mRNA levels (Figure 6A). No difference was observed in the CaMKII mRNA levels between the groups. Western blotting was performed to evaluate the expression levels of these proteins. As shown in Figure 6B and C, Cx43 and Cx40 were downregulated in AIC rats, but only Cx43 expression was restored after EA treatment. Our results indicated that EA selectively restores Cx43 expression, revealing that it reverses AF-induced electrical remodeling by re-establishing intercellular conductive pathways. This restoration normalized the CV and reduced the formation of arrhythmogenic substrates

(Figure 6D). We also observed a significant upregulation of CaMKII in rats with the AIC phenotype, which EA treatment effectively prevented by EA treatment (Figure 6B and C). Collectively, our results show that AIC causes changes in the expression of proteins related to electrical propagation and intracellular calcium handling in the myocardium. The expression levels of Cx43 and CaMKII may contribute to the protective effect of EA treatment at BL15 on AIC (Figure 6D).

Discussion

In this study, we used ACh-CaCl₂ to induce AF caused by AIC in SD rats with P-wave disappearance on ECG, as

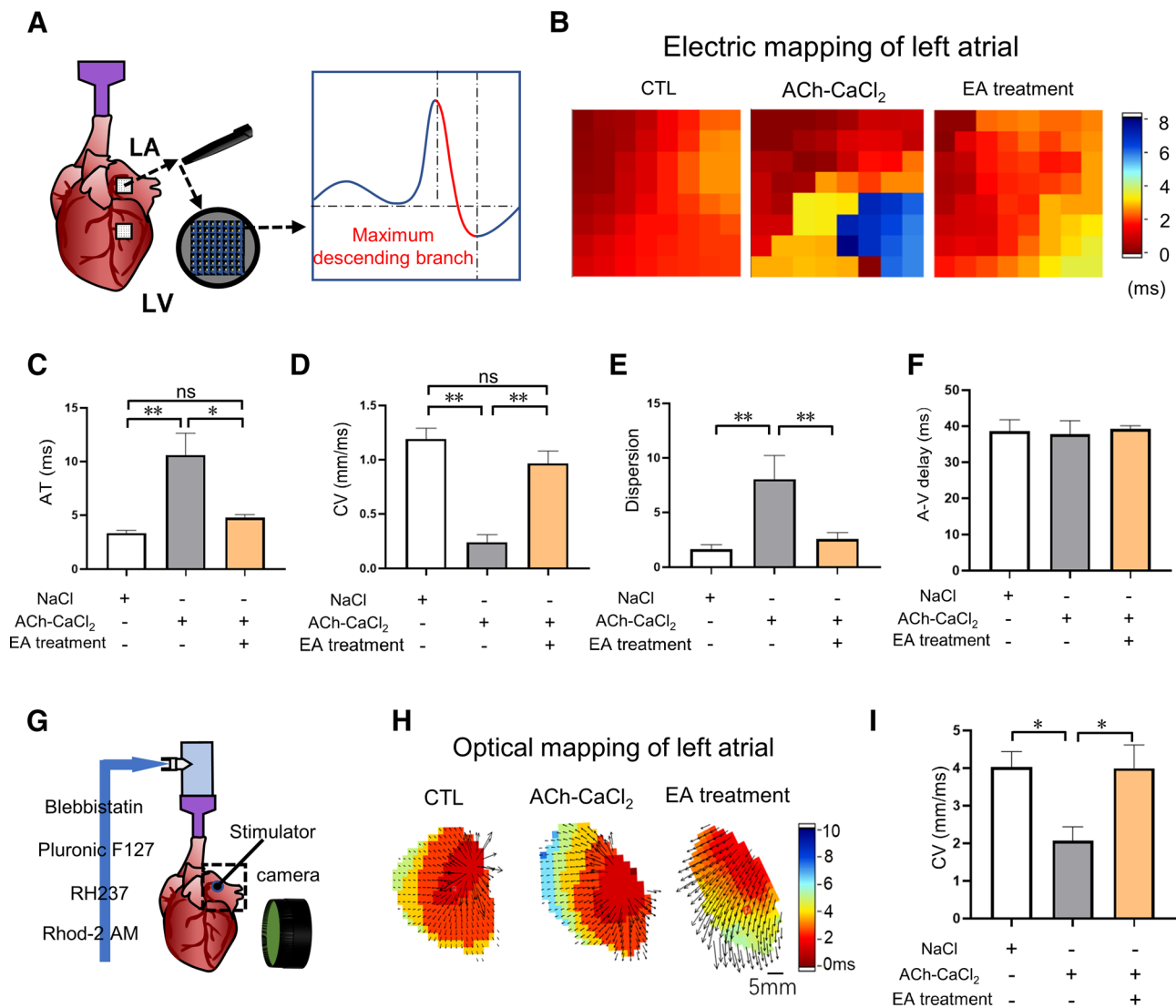


Figure 3. Effect of EA treatment on atrial conduction using electrical and optical mapping. (A) Setups of the Langendorff perfusion system and electrical mapping recording of the LA and LV. (B) Conduction isochrone map of the control, ACh + CaCl₂, and EA treatment groups in the left atrium under 5 Hz stimulation. (C) Conduction time, (D) CV, (E) conduction dispersion, and (F) atrial-ventricular delay of the control, ACh + CaCl₂, and EA treatment groups in the left atrium under 5 Hz stimulation. AIC modeling prolonged AT and dispersion and shortened CV, whereas EA treatment reversed these effects. Notably, neither AIC modeling nor EA treatment affected AV conduction. (G) Optical mapping of the atrial setup under the Langendorff perfusion system and sequence of dye addition. (H) Representative isochrone map of conduction in the left atrium measured by optical mapping under 5 Hz stimulation. (I) CV of the control, ACh + CaCl₂, and EA treatment groups in the left atrium under 5 Hz stimulation. AIC modeling did not prolong the rise time of phase 0 and dispersion of cardiac action potential, and EA had no effect on the modeled rat heart. AIC modeling shortened the CV, and EA treatment reversed the above effect in the modeled rat heart, and both changes were significantly different. $n = 6$ in all groups, * $P < 0.05$, ** $P < 0.01$. ACh: Acetylcholine; AIC: Arrhythmia-induced cardiomyopathy; AT: Atrial conduction time; CV: Conduction velocity; EA: Electroacupuncture; LA: Left atrium; LV: Left ventricle; ns: No significant difference between groups.

previously reported^[34]. The model rats presented typical AIC characteristics: (1) some degree of cardiac systolic or diastolic dysfunction, (2) ventricular dilation by standard echocardiographic evaluation, and (3) arrhythmia as the only cause of cardiomyopathy [Figure 1; Supplementary Figures S1 and S2, <https://links.lww.com/AHM/A185> and <https://links.lww.com/AHM/A186>]. Furthermore, after treatment with Amio in our AIC rat model, the functional properties of the myocardium were partially or completely restored in the treated groups. These results indicate that the arrhythmia model used in our study is a suitable AIC model for cardiomyopathy research. However, the pathophysiological mechanisms underlying AIC are unclear. In patients with cardiomyopathy, the parasympathetic

regulation of heart rate is impaired, and decreased cardiac function caused by cardiomyopathy increases the heart rate in a compensatory manner^[50]. In addition, our study provided evidence, for the first time, of changes in cardiac conduction and calcium handling in the ACh-CaCl₂ model group using electrical and optical mapping (Figure 3C and I). Consistently, another study showed that AF initiation requires slow conduction at a high heart rate^[12]. Furthermore, changes in both action potential duration (APD) and CV contribute to abnormal conduction and proarrhythmic substrates in AIC hearts^[17,51]. We combined electrical and optical mapping for the first time to provide additional evidence supporting the association between cardiac arrhythmia and cardiomyopathy.

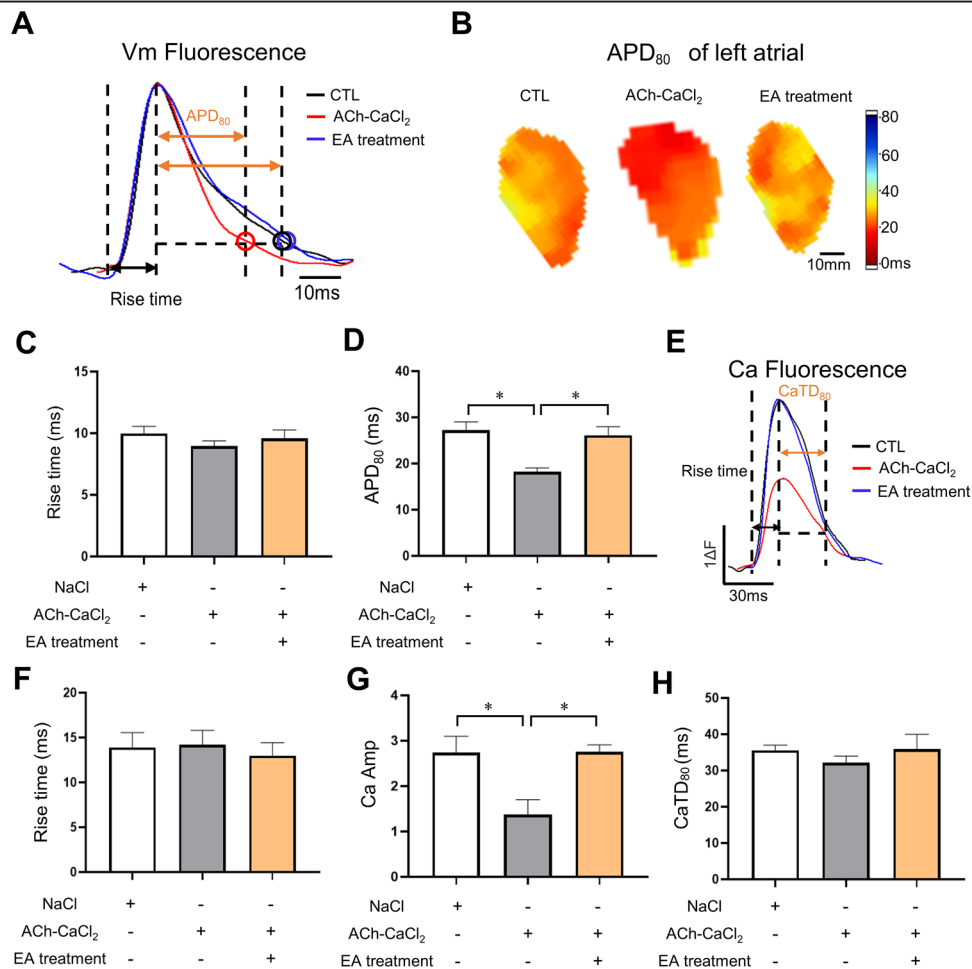


Figure 4. Changes in APD_{80} and intracellular calcium concentrations throughout the left atrium were detected by optical mapping. (A) Representative trace and measurement of APD_{80} in the left atrium measured by optical mapping under 5 Hz stimulation. (B) Representative isochrone map of APD_{80} of the left atrium measured by optical mapping under 5 Hz stimulation. Statistics of (C) rise time and (D) APD_{80} in the left atrium measured by optical mapping under 5 Hz stimulation. APD_{80} was shortened because of AF modeling compared with the control group, and EA treatment reversed APD_{80} . (E) Representative trace of the intracellular calcium concentration in the left atrium measured by optical mapping under 5 Hz stimulation. (F) Rise time, (G) peak amplitude of intracellular Ca release, and (H) $CaTD_{80}$ of the control, ACh + $CaCl_2$, and EA treatment groups in the left atrium under 5 Hz stimulation. AIC modeling did not prolong the rise time or $CaTD_{80}$ of calcium release, and EA had no effect on the modeled rat heart. Notably, in the ACh + $CaCl_2$ group, the peak amplitude of intracellular Ca release decreased, and EA treatment reversed the decrease in the modeled rat heart, and both changes were significantly different. $n = 6$ in all groups, $*P < 0.05$. ACh: Acetylcholine; AF: Atrial fibrillation; AIC: Arrhythmia-induced cardiomyopathy; APD_{80} : Action potential duration 80; EA: Electroacupuncture; ns: No significant difference between groups.

Therapeutic effects of EA at BL15, sham EA, ST25, and Amio. Our results revealed that EA at BL15 not only alleviated arrhythmias and improved cardiac function but also reversed ventricular structural remodeling. In contrast, Amio partially restored the hemodynamic parameters. This distinction shows that EA at BL15 may exert its effects through multi-target mechanisms, rather than solely suppressing electrical activity. Previous studies have shown that effective acupuncture treatment for cardiovascular diseases often involves acupoints closely associated with cardiac regulation, such as Neiguan (PC6) and Shenmen (HT7)^[52]. Xinshu (BL15), a back-shu point, is directly linked to heart function regulation according to traditional Chinese medicine (TCM) theory and is widely used in treating cardiovascular conditions^[53]. In our study, we selected Tianshu (ST25) as the control point because of its clinical use in gastrointestinal disorders^[54]. The absence of cardioprotective effects of ST25 against AIC reinforces the specificity and therapeutic relevance of acupoint selection in this study.

Moreover, compared to acupoints such as PC6, BL15 is anatomically positioned at the T5 spinal nerve segment level. This location may allow more direct modulation of cardiac autonomic nerve activity and electrophysiological stability through the spinal cord-sympathetic nerve pathway, potentially explaining its superior effectiveness. Amio, a broad-spectrum antiarrhythmic agent, primarily suppresses AF by blocking potassium channels to prolong the action potential duration, inhibiting β -adrenergic receptors, and suppressing the calcium channels^[55]. However, despite its potent antifibrillatory effects, its ability to reverse ventricular remodeling is limited.

Our results also indicate that AIC caused by AF may be closely related to cardiac conduction injuries. Here, we discovered that the increased inducibility and sustained duration of AF were alleviated by EA at the BL15 acupoint (Figure 2E–G), which can be explained by the shortened and restored APD_{80} in AIC rats and the EA treatment group (Figure 4C). This notion is supported by previous studies in which AF caused electrical

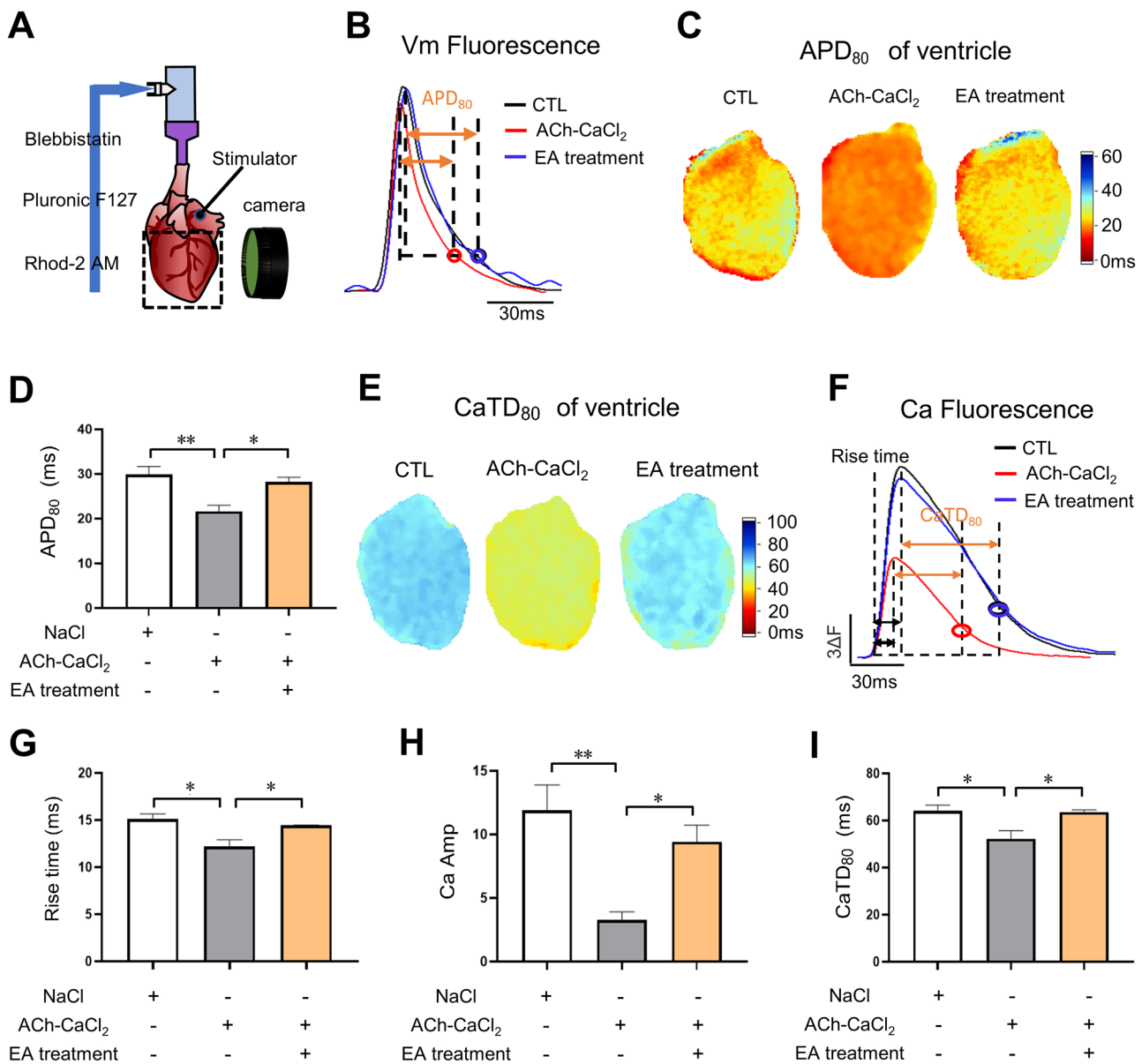


Figure 5. Changes in APD₈₀ and intracellular calcium release in rat ventricles as detected by optical mapping. (A) Setup of the Langendorff perfusion system and optical mapping recording of the rat ventricle. (B) Representative isochrone map and (C) trace of action potential recorded by optical mapping under 5 Hz stimulation. (D) APD₈₀ of the ventricle measured by optical mapping under 5 Hz stimulation. APD₈₀ was shortened in the model group compared with the control group, whereas EA treatment in the BL15 group restored APD₈₀ to the level of the control group. (E) Representative isochrone map and (F) real-time calcium fluorescence amplitude trace of intracellular calcium release recorded by optical mapping under 5 Hz stimulation. (G) Rise time, (H) peak amplitude of intracellular Ca release, and (I) CaTD₈₀ of the control, ACh + CaCl₂, and EA treatment groups in the ventricle under 5 Hz stimulation. AF modeling did not prolong the rise time or CaTD₈₀ of Calcium release, and EA did not affect the modeled rat ventricle. Notably, in the ACh + CaCl₂ group, the peak amplitude of intracellular Ca release decreased in the rat ventricle, and EA treatment at BL15 reversed the decrease in the ACh + CaCl₂ group, and both changes showed significant differences. $n = 6$ in all groups, $*P < 0.05$, $**P < 0.01$. ACh: Acetylcholine; AF: Atrial fibrillation; APD₈₀: Action potential duration 80; EA: Electroacupuncture; ns: No significant difference between groups.

remodeling of the myocardium in both humans and rats^[56–57]. Furthermore, the CV of myocardial electrical signals and the dispersion of repolarization in the isolated rat heart by electrical mapping confirmed that the CV decreased in the AIC and increased in the dispersion (Figure 3A–C). Previous studies have linked the reduced expression of atrial connexins (such as Cx40 and Cx43) to electrical propagation impairment, which leads to a proarrhythmic substrate and AF^[58–60]. Cx43 is the principal gap junction protein in cardiomyocytes and is typically localized at intercalated discs, where it ensures directional electrical conduction along the longitudinal

axis of the cardiomyocytes and throughout the cardiac tissue. Downregulation of Cx43 reduces its expression in intercalated discs, leading to fewer gap junctions. This impairs the electrical coupling between cardiomyocytes and slows the propagation of electrical impulses^[61–62]. Consistently, the recovery of Cx43 expression can explain the restoration of electrical CV in myocardial tissue (Figure 6). Collectively, our findings raise the possibility that EA treatment at BL15 improves the CV of cardiac electrical signals and is associated with an increase in Cx43 expression, which may contribute to the prevention of AF-induced cardiac electrical remodeling (Figure 6D).

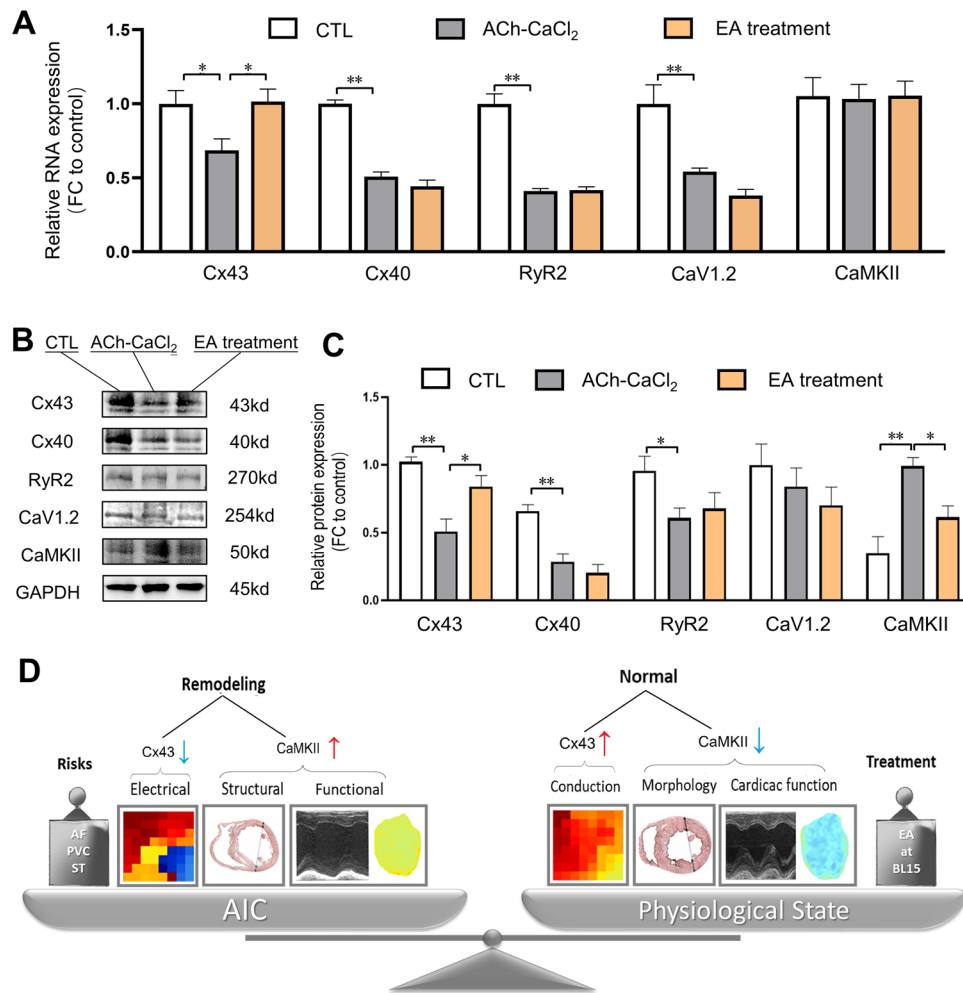


Figure 6. Changes in gene expression in AIC ventricular myocardium with/without EA treatment. (A) Statistical results of qPCR for Cx43, Cx40, RyR2, CaV1.2, and CaMKII in each group expressed in the rat ventricle. (B) Representative Western blot images of Cx43, Cx40, RyR2, CaV1.2, and CaMKII expressed in rat ventricular myocardia. The bands in each panel from left to right are the control, ACh-CaCl₂, and EA treatment groups, respectively. (C) Statistical results of Western blotting of the proteins expressed in the rat ventricle in each group. (D) Schematic representation of the effect of EA treatment at BL15 on recovering cardiac remodeling caused by the risk of arrhythmias. * $P < 0.05$, ** $P < 0.01$. ACh: Acetylcholine; AF: Atrial fibrillation; AIC: Arrhythmia-induced cardiomyopathy; EA: Electroacupuncture; PVC: Premature ventricular contraction.

The coordinated movement of Ca²⁺ between the cytosol and SR is necessary for cardiomyocyte contraction^[21]. CaMKII upregulation plays a key role in disrupting myocardial calcium homeostasis. CaMKII phosphorylates the cardiac ryanodine receptor (RyR), significantly increasing its opening probability and causing aberrant calcium leakage from the SR. This leakage depletes SR calcium stores, weakens myocardial contractility, and induces calcium waves. These waves activate the sodium-calcium exchanger (NCX), generating delayed after-depolarization and promoting arrhythmogenesis^[63–64]. AIC is typically associated with defects in myocardial Ca²⁺ transients and Ca²⁺ handling^[65]. In the current study, AIC significantly increased the VLIDs (Figure 1E) and LVIDd (Figure 1F), indicating a larger volume in the systolic period, leading to decreased EF (Figure 1C) and FS (Figure 1D). However, abnormal electrical conduction of the AIC was insufficient to explain the decrease in cardiac contractile function in the rat heart, as the rhythm of the atrium could not impact the contraction force to such an extent during systole (Figure 1B). Furthermore, our optical mapping results revealed that

EA treatment prevented the AF-induced decrease in intracellular calcium activity in atrial myocytes caused by AF (Figure 4E). Previous studies have consistently shown that loss of atrial function can lead to a decrease in ventricular output, which partially recovers after restoring sinus rhythm^[2,20]. Myocardial contractility is positively correlated with the concentration of intracellular calcium^[49]. A similar phenomenon also occurred in the ventricles; the concentration of intracellular calcium also decreased, but with a lower CaTD₈₀ in the ventricle (Figure 5H and I). These results indicate a certain level of disorder in calcium handling as well as injury to cardiac conduction in AIC hearts, which can be restored.

In this study, we observed that EA treatment significantly improved cardiac function and electrophysiological parameters in the AIC model. However, certain indicators, such as ventricular CaTD₈₀ and Cx40 protein expression, were not completely normalized to control levels. In addition, although CaMKII protein expression was significantly elevated in the AIC group and reduced following EA treatment, CaMKII mRNA levels did not change. These discordant findings may

reflect several underlying mechanisms of action. (1) Post-transcriptional regulation and time-dependent effects: Asynchronous changes between mRNA and protein levels are common during pathological repair. CaMKII activation may result from enhanced translational efficiency or post-translational modifications, such as phosphorylation, rather than transcriptional upregulation. (2) Pathological compensation and residual injury: The partial recovery of ventricular $CaTD_{80}$ may indicate persistent damage to the calcium-handling systems in the AIC model, such as mitochondrial calcium overload or irreversible downregulation of SR calcium pump function, which EA at BL15 may not be fully reversed.

Notably, the mechanisms underlying the EA-mediated improvement of AIC may involve its anti-inflammatory and antioxidant properties. Emerging evidence has shown that inflammatory responses contribute to AF by promoting abnormal calcium release from the SR, shortening the ERP of the atrium, and inducing atrial hypertrophy^[66]. Reactive oxygen species (ROS) disrupt calcium homeostasis by oxidatively modifying the methionine residues of CaMKII, thereby driving pathological hyperactivation^[67]. Acupuncture suppresses both oxidative stress and inflammation, thereby providing cardioprotective effects in various cardiovascular disease models^[68–69].

Building on these findings, future studies should quantify myocardial levels of NLRP3 inflammasomes, ROS, and additional oxidative stress markers to further elucidate the multi-target mechanisms through which EA mitigates AIC. However, this study had several limitations. Although our optical mapping data revealed synchronized improvements in calcium transients and APD_{80} levels following EA treatment (Figures 4 and 5), the mechanistic relationship between these parameters remains unclear. Specifically, future investigations should determine whether shortened APD directly contributes to calcium-handling dysfunction in the AIC or whether impaired calcium handling precipitates APD changes, how EA-mediated modulation of CaMKII (Figure 6) orchestrates the observed electrophysiological, and calcium regulatory improvements. Employing advanced techniques, such as high temporal resolution and simultaneous voltage calcium imaging, may help resolve this temporal relationship. Furthermore, although our data linked the altered expression of Cx43 and CaMKII to the therapeutic effects of EA, a causal relationship has not yet been established *in vivo*. Future studies should use molecular interventions, such as gene knockouts or overexpression models, to validate the necessity and sufficiency of these targets in mediating the effects of EA on AIC development.

Conclusion

Our study provided a rat model of AIC with AF symptoms and reversible dilated cardiomyopathy (DCM). Our results also revealed the critical role of EA treatment at BL15 in effectively treating AIC by reversing the above symptoms, particularly by improving functional indices linked to cardiac morphological recovery, such as ventricular dilation and wall thinning. The mechanisms underlying the pathophysiology and treatment of AIC

with EA involve electrical conduction and calcium handling in the myocardium. Collectively, this study contributes to the understanding of the cardioprotective effects of acupuncture therapy and provides novel strategies for the clinical management of AIC.

Conflict of interest statement

The authors declare no conflict of interest.

Funding

This work was supported by the National Key R&D Program of China (2022YFC3500405, 2019YFC1712105); The National Science Foundation of China (82374075); The National Comprehensive Traditional Chinese Medicine Reform Demonstration Zone Science and Technology Collaborative Development Project (GZY-KJS-SD-2024-046); Taishan Scholar Youth Project of Shandong Province (tsqn202306188).

Author contributions

Shengxuan Sun, Jing Huang, and Yijun Hu wrote the original draft and conducted formal analysis. Yang Su, Huanhuan Yu, and Feng Guo contributed to software, methodology, and data curation. Meng Zhang, Yucen Xia, and Lin Yao conducted formal analysis and curated data. Taiyi Wang and Yongjun Chen reviewed and edited the manuscript, performed validation, supervised the study, acquired funding, and conceptualized the research. All of the authors have read and approved the published version of the manuscript.

Ethical approval of studies and informed consent

This animal study was approved by the Institutional Animal Care and Use Committee of the Guangzhou University of Chinese Medicine, ethical review approval number: 20201124005.

Acknowledgments

We thank Jingya Wang (Guangzhou University of Chinese Medicine, Guangzhou, China) for technical support on small-animal ultrasound imaging.

Data availability

All data generated or analyzed during this study are included in this published article.

References

- [1] Bozkurt B, Colvin M, Cook J, et al. Current diagnostic and treatment strategies for specific dilated cardiomyopathies: a scientific statement from the American Heart Association. *Circulation* 2016;134(23):e579–e646.
- [2] Sossalla S, Vollmann D. Arrhythmia-induced cardiomyopathy. *Deutsches Arzteblatt Int* 2018;115(19):335–341.
- [3] Brembilla-Perrot B, Ferreira JP, Manenti V, et al. Predictors and prognostic significance of tachycardiomyopathy: insights from a cohort of 1269 patients undergoing atrial flutter ablation. *Eur J Heart Fail* 2016;18(4):394–401.
- [4] Carballeira Pol L, Deyell MW, Frankel DS, et al. Ventricular premature depolarization QRS duration as a new marker of risk for the development of ventricular premature depolarization-induced cardiomyopathy. *Heart Rhythm* 2014;11(2):299–306.

- [5] Ju W, Yang B, Li M, et al. Tachycardiomyopathy complicated by focal atrial tachycardia: incidence, risk factors, and long-term outcome. *J Cardiovasc Electrophysiol* 2014;25(9):953–957.
- [6] Umana E, Solares CA, Alpert MA. Tachycardia-induced cardiomyopathy. *Am J Med* 2003;114(1):51–55.
- [7] Nuzzi V, Cannatà A, Manca P, et al. Atrial fibrillation in dilated cardiomyopathy: outcome prediction from an observational registry. *Int J Cardiol* 2021;323:140–147.
- [8] Huizar JF, Ellenbogen KA, Tan AY, et al. Arrhythmia-induced cardiomyopathy: JACC State-of-the-Art Review. *J Am Coll Cardiol* 2019;73(18):2328–2344.
- [9] Connolly SJ. Evidence-based analysis of amiodarone efficacy and safety. *Circulation* 1999;100(19):2025–2034.
- [10] Mujović N, Marinković M, Lenarczyk R, et al. Catheter ablation of atrial fibrillation: an overview for clinicians. *Adv Ther* 2017;34(8):1897–1917.
- [11] Van Erven L, Schalijs MJ. Amiodarone: an effective antiarrhythmic drug with unusual side effects. *Heart (British Cardiac Society)* 2010;96(19):1593–1600.
- [12] Lalani GG, Schricker A, Gibson M, et al. Atrial conduction slows immediately before the onset of human atrial fibrillation: a bi-atrial contact mapping study of transitions to atrial fibrillation. *J Am Coll Cardiol* 2012;59(6):595–606.
- [13] Kato T, Iwasaki YK, Nattel S. Connexins and atrial fibrillation: filling in the gaps. *Circulation* 2012;125(2):203–206.
- [14] Saffitz JE. Connexins, conduction, and atrial fibrillation. *N Engl J Med* 2006;354(25):2712–2714.
- [15] Kanagaratnam P, Rothery S, Patel P, et al. Relative expression of immunolocalized connexins 40 and 43 correlates with human atrial conduction properties. *J Am Coll Cardiol* 2002;39(1):116–123.
- [16] Narayan SM, Franz MR, Clopton P, et al. Repolarization alternans reveals vulnerability to human atrial fibrillation. *Circulation* 2011;123(25):2922–2930.
- [17] Narayan SM, Kazi D, Krummen DE, et al. Repolarization and activation restitution near human pulmonary veins and atrial fibrillation initiation: a mechanism for the initiation of atrial fibrillation by premature beats. *J Am Coll Cardiol* 2008;52(15):1222–1230.
- [18] Bers DM. Cardiac excitation-contraction coupling. *Nature* 2002;415(6868):198–205.
- [19] Simantirakis EN, Koutalas EP, Vardas PE. Arrhythmia-induced cardiomyopathies: the riddle of the chicken and the egg still unanswered? *Europace* 2012;14(4):466–473.
- [20] Gopinathannair R, Etheridge SP, Marchlinski FE, et al. Arrhythmia-induced cardiomyopathies: mechanisms, recognition, and management. *J Am Coll Cardiol* 2015;66(15):1714–1728.
- [21] Kho C, Lee A, Hajjar RJ. Altered sarcoplasmic reticulum calcium cycling—targets for heart failure therapy. *Nat Rev Cardiol* 2012;9(12):717–733.
- [22] Raymond-Paquin A, Nattel S, Wakili R, et al. Mechanisms and clinical significance of arrhythmia-induced cardiomyopathy. *Can J Cardiol* 2018;34(11):1449–1460.
- [23] Lomuscio A, Bellelli S, Battezzati PM, et al. Efficacy of acupuncture in preventing atrial fibrillation recurrences after electrical cardioversion. *J Cardiovasc Electrophysiol* 2011;22(3):241–247.
- [24] Yan YH, Li BX, Wu LY. Clinical observation of paroxysmal atrial fibrillation treated with a combination of acupuncture and medicine. *Zhejiang J Tradit Chin Med* 2014;49(11):833.
- [25] Li W, Li Z, Zhang H, et al. Acupoint catgut embedding for insomnia: a meta-analysis of randomized controlled trials. *Evid Based Complement Altern Med* 2020;2020:5450824.
- [26] Wu SB, Cao J, Gao F, et al. Effect of electroacupuncture on expression of myocardial PI 3K, HIF-1 α and VEGF in rats with cerebral-cardiac syndrome. *Zhen Ci Yan Jiu* 2013;38(2):87–92.
- [27] Hao F, Liu L, Wu ZJ, et al. Effect of electroacupuncture at different acupoints on expression of NGF and TrkA in cerebral cortex in rats with myocardial ischemia. *Zhen Ci Yan Jiu* 2018;43(7):400–405.
- [28] Gao Z, Hu S, Wang ZJ, et al. Treating coronary heart disease by acupuncture at neiguan (PC6) and xinahu (BL15): an efficacy assessment by SPECT. *Zhongguo Zhong Xi Yi Jie He Za Zhi* 2013;33(9):1196–1198.
- [29] Deng YJ, Liang WX, Cheng SY. Influence of acupoint-catgut implantation on blood pressure and cardiac function in chronic congestive heart failure rats. *Zhen Ci Yan Jiu* 2011;36(1):40–45.
- [30] Huang J, Yan JL, Wang TY, et al. Research progress on central autonomic nervous mechanism of acupuncture at Neiguan point in the treatment of atrial fibrillation. *Acupuncture Herbal Med* 2023;3(3):149–157.
- [31] Liu CZ. Relationship between acupuncture and the autonomic nervous system. *Acupuncture Herbal Med* 2023;3(3):137–138.
- [32] Lee NR, Kim SB, Heo H, et al. Comparison of the effects of manual acupuncture, laser acupuncture, and electromagnetic field stimulation at acupoint point BL15 on heart rate variability. *J Acupunct Meridian Studies* 2016;9(5):257–263.
- [33] Wei W, Qingling LI, Qiang MA, et al. Effects of moxibustion at bilateral Feishu (BL13) and Xinshu (BL15) combined with benazepril on myocardial cells apoptosis index and apoptosis-related proteins cytochrome c and apoptosis-inducing factor in rats with chronic heart failure. *J Traditional Chin Med* 2022;42(2):227–233.
- [34] Zou D, Geng N, Chen Y, et al. Ranolazine improves oxidative stress and mitochondrial function in the atrium of acetylcholine-CaCl₂ induced atrial fibrillation rats. *Life Sci* 2016;156:7–14.
- [35] Wang J, Zhang Q, Yao L, et al. Modulating activity of PVN neurons prevents atrial fibrillation induced circulation dysfunction by electroacupuncture at BL15. *Chin Med* 2023;18(1):135.
- [36] Du XJ, Esler MD, Dart AM. Sympatholytic action of intravenous amiodarone in the rat heart. *Circulation* 1995;91(2):462–470.
- [37] Yang X, Zhang L, Liu H, et al. Cardiac sympathetic denervation suppresses atrial fibrillation and blood pressure in a chronic intermittent hypoxia rat model of obstructive sleep apnea. *J Am Heart Assoc* 2019;8(4):e010254.
- [38] Chan YH, Chang GJ, Lai YJ, et al. Atrial fibrillation and its arrhythmogenesis associated with insulin resistance. *Cardiovasc Diabetol* 2019;18(1):125.
- [39] Reil JC, Hohl M, Selejan S, et al. Aldosterone promotes atrial fibrillation. *Eur Heart J* 2012;33(16):2098–2108.
- [40] Hiram R, Naud P, Xiong F, et al. Right atrial mechanisms of atrial fibrillation in a rat model of right heart disease. *J Am Coll Cardiol* 2019;74(10):1332–1347.
- [41] Wu Q, Liu H, Liao J, et al. Colchicine prevents atrial fibrillation promotion by inhibiting IL-1 β -induced IL-6 release and atrial fibrosis in the rat sterile pericarditis model. *Biomed Pharmacother* 2020;129:110384.
- [42] Choi EK, Chang PC, Lee YS, et al. Triggered firing and atrial fibrillation in transgenic mice with selective atrial fibrosis induced by overexpression of TGF- β 1. *Circ J* 2012;76(6):1354–1362.
- [43] Umar S, Lee JH, De Lange E, et al. Spontaneous ventricular fibrillation in right ventricular failure secondary to chronic pulmonary hypertension. *Circ Arrhythm Electrophysiol* 2012;5(1):181–190.
- [44] Lang D, Glukhov AV. High-resolution optical mapping of the mouse sino-atrial node. *J Vis Exp* 2016;118(118):e54773.
- [45] Yu WC, Chen SA, Lee SH, et al. Tachycardia-induced change of atrial refractory period in humans: rate dependency and effects of antiarrhythmic drugs. *Circulation* 1998;97(23):2331–2337.
- [46] Kalifa J, Tanaka K, Zaitsev AV, et al. Mechanisms of wave fractionation at boundaries of high-frequency excitation in the posterior left atrium of the isolated sheep heart during atrial fibrillation. *Circulation* 2006;113(5):626–633.
- [47] Spector P. Principles of cardiac electric propagation and their implications for re-entrant arrhythmias. *Circ Arrhythm Electrophysiol* 2013;6(3):655–661.
- [48] Weiss JN, Qu Z, Chen PS, et al. The dynamics of cardiac fibrillation. *Circulation* 2005;112(8):1232–1240.
- [49] Eisner DA, Caldwell JL, Kistamás K, et al. Calcium and excitation-contraction coupling in the heart. *Circ Res* 2017;121(2):181–195.
- [50] Braunwald E. Cardiomyopathies: an overview. *Circ Res* 2017;121(7):711–721.
- [51] Anyukhovsky EP, Sosunov EA, Plotnikov A, et al. Cellular electrophysiological properties of old canine atria provide a substrate for arrhythmogenesis. *Cardiovasc Res* 2002;54(2):462–469.
- [52] Cai Y, Zhang CS, Liu S, et al. Acupuncture for premature ventricular complexes without ischemic or structural heart diseases: a systematic review and meta-analysis of clinical and pre-clinical evidence. *Front Med* 2022;9:1019051.
- [53] Hsu CC, Weng CS, Liu TS, et al. Effects of electrical acupuncture on acupoint BL15 evaluated in terms of heart rate variability, pulse rate variability and skin conductance response. *Am J Chin Med* 2006;34(1):23–36.
- [54] Zhang L, Yu C, Chen B, et al. Corrigendum: Modulation of colonic function in irritable bowel syndrome rats by electroacupuncture at ST25 and the neurobiological links between ST25 and the colon. *Front Neurosci* 2023;17:1177384.
- [55] Kirchhof P, Benussi S, Kotecha D, et al. 2016 ESC Guidelines for the management of atrial fibrillation developed in collaboration with EACTS. *Eur J Cardio Thorac Surg* 2016;50(5):e1–e88.

- [56] Bohne LJ, Jansen HJ, Daniel I, et al. Electrical and structural remodeling contribute to atrial fibrillation in type 2 diabetic db/db mice. *Heart rhythm* 2021;18(1):118–129.
- [57] Lee HC. Electrical remodeling in human atrial fibrillation. *Chin Med J (Engl)* 2013;126(12):2380–2383.
- [58] Nattel S, Heijman J, Zhou L, et al. Molecular basis of atrial fibrillation pathophysiology and therapy: a translational perspective. *Circ Res* 2020;127(1):51–72.
- [59] Nao T, Ohkusa T, Hisamatsu Y, et al. Comparison of expression of connexin in right atrial myocardium in patients with chronic atrial fibrillation versus those in sinus rhythm. *Am J Cardiol* 2003;91(6):678–683.
- [60] Gemel J, Levy AE, Simon AR, et al. Connexin40 abnormalities and atrial fibrillation in the human heart. *J Mol Cell Cardiol* 2014;76:159–168.
- [61] Smyth JW, Hong TT, Gao D, et al. Limited forward trafficking of connexin 43 reduces cell-cell coupling in stressed human and mouse myocardium. *J Clin Invest* 2010;120(1):266–279.
- [62] Wahl CM, Schmidt C, Hecker M, et al. Distress-mediated remodeling of cardiac connexin-43 in a novel cell model for arrhythmogenic heart diseases. *Int J Mol Sci* 2022;23(17):10174.
- [63] Curran J, Brown KH, Santiago DJ, et al. Spontaneous Ca waves in ventricular myocytes from failing hearts depend on Ca(2+)-calmodulin-dependent protein kinase II. *J Mol Cell Cardiol* 2010;49(1):25–32.
- [64] Anderson ME. Oxidant stress promotes disease by activating CaMKII. *J Mol Cell Cardiol* 2015;89(Pt B):160–167.
- [65] Cory CR, Mccutcheon LJ, O'grady M, et al. Compensatory downregulation of myocardial Ca channel in SR from dogs with heart failure. *Am J Physiol* 1993;264(3 Pt 2):H926–H937.
- [66] Yao C, Veleva T, Scott L, JR, et al. Enhanced cardiomyocyte NLRP3 inflammasome signaling promotes atrial fibrillation. *Circulation* 2018;138(20):2227–2242.
- [67] Erickson JR, Joiner ML, Guan X, et al. A dynamic pathway for calcium-independent activation of CaMKII by methionine oxidation. *Cell* 2008;133(3):462–474.
- [68] Wang M, Pan W, Xu Y, et al. Microglia-mediated neuroinflammation: a potential target for the treatment of cardiovascular diseases. *J Inflamm Res* 2022;15:3083–3094.
- [69] Zhang J, Zhu L, Li H, et al. Electroacupuncture pretreatment as a novel avenue to protect heart against ischemia and reperfusion injury. *Evid Based Complement Alternative Med* 2020;2020:9786482.